Thin Solid Films 591 (2015) 66–71

Contents lists available at ScienceDirect

Thin Solid Films

journal homepage: www.elsevier.com/locate/tsf

Integration of epitaxial $Pb(Zr_{0.52}Ti_{0.48})O_3$ films on GaN/AlGaN/GaN/Si(111) substrates using rutile TiO_2 buffer layers

K. Elibol [a], M.D. Nguyen [a,b,c], R.J.E. Hueting [a], D.J. Gravesteijn [a,d], G. Koster [a,*], G. Rijnders [a]

[a] MESA + Institute for Nanotechnology, University of Twente, P.O. Box 217, 7500AE Enschede, The Netherlands
[b] SolMateS B.V., Drienerlolaan 5, Building 6, 7522NB Enschede, The Netherlands
[c] International Training Institute for Materials Science, Hanoi University of Science and Technology, No.1 Dai Co Viet road, Hanoi 10000, Viet Nam
[d] NXP Semiconductors Research, High Tech Campus 46, 5656AE Eindhoven, The Netherlands

ARTICLE INFO

Article history:
Received 30 September 2014
Received in revised form 17 June 2015
Accepted 21 July 2015
Available online 30 July 2015

Keywords:
Lead zirconate titanate
Gallium nitride
Rutile titanium dioxide
Heterostructures
Thin film optimization
Structural properties
Ferroelectric properties
Pulsed laser deposition

ABSTRACT

The integration of ferroelectric layers on gallium nitride (GaN) offers a great potential for various applications. Lead zirconate titanate (PZT), in particular $Pb(Zr_{0.52}Ti_{0.48})O_3$, is an interesting candidate. For that a suitable buffer layer should be grown on GaN in order to prevent the reaction between PZT and GaN, and to obtain PZT with a preferred orientation and phase. Here, we study pulsed laser deposited (100) rutile titanium oxide (R-TiO_2) as a potential buffer layer candidate for ferroelectric PZT. For this purpose, the growth, morphology and the surface chemical composition of R-TiO_2 films were analyzed by reflection high-energy electron diffraction, atomic force microscopy, X-ray diffraction, and X-ray photoelectron spectroscopy. We find optimally (100) oriented R-TiO_2 growth on GaN (0002) using a 675 °C growth temperature and 2 Pa O_2 deposition pressure as process conditions. More importantly, the R-TiO_2 buffer layer grown on GaN/Si substrates prevents the unwanted formation of the PZT pyrochlore phase. Finally, the remnant polarization and coercive voltage of the PZT film on TiO_2/GaN/Si with an interdigitated-electrode structure were found to be 25.6 μC/cm^2 and 8.1 V, respectively.

1. Introduction

The epitaxial integration of ferroelectric films on GaN enables several new applications [1]. Ferroelectric materials such as lead zirconate titanate (PZT or $Pb[Zr_xTi_{1-x}]O_3$) can pave the way for new device concepts due to the unique intrinsic ferroelectric properties of this material, such as a large remnant polarization, a large dielectric constant, good piezoelectric and pyroelectric response, fast switching speed and a high Curie temperature [2,3]. These materials have a high potential for non-volatile memories, high-density capacitors, actuators, and sensors [4–7]. Another possibility of the integration of PZT is the possibility to reduce the power consumption in transistors with gallium nitride (GaN) as the platform. There has been a strong drive for steep-subthreshold slope devices such as ferroelectric field-effect transistors (FeFETs) to reduce the leakage current. FeFETs are basically metal–insulator–semiconductor transistors comprising a ferroelectric layer as a (part of a) gate insulator [8–11]. In particular PZT close to the morphotropic phase boundary ($PbZr_xTi_{1-x}O_3$, $x = 0.52$) should be very suitable for FeFET applications [12,13].

GaN (a III–V semiconductor) is an important material with many potential applications such as field effect transistors in high power and high frequency devices, and light emitters due to its direct, wide band gap of 3.45 eV at room temperature [14–17]. Moreover it possesses a high chemical and mechanical stability and high thermal conductivity [18]. In addition, presently more and more GaN is integrated on silicon substrates, because of its large size availability, mass production, and hence significantly lower cost for GaN optoelectronic and microelectronic devices [19]. The GaN films are grown on Si (111) substrates to obtain favorable lattice match conditions between GaN and Si because GaN has a hexagonal symmetry.

Recently, the integration of PZT with GaN has attracted the attention in the scientific community despite the difficulties to integrate these two materials [20,21]. There is limited experience with the integration of PZT material on GaN, mainly because of the different crystal structures and large lattice mismatch between that of perovskite PZT and wurtzite GaN [22,23]. PZT films grown directly on GaN can react with GaN, hence, the interdiffusion of Pb and Ti atoms at the PZT/GaN interface could occur and in addition a pyrochlore phase of PZT is formed [24]. In order to overcome this interdiffusion problem, a so-called buffer layer can be used between PZT and GaN layer [22]. A buffer layer reduces the interdiffusion and avoids direct reaction between the ferroelectric and the semiconductor. It can also be effective to promote certain growth orientation of PZT films and to avoid ferroelectric performance degradation [25]. Earlier reports [20,22,23,26,27] mainly focused on the integration of epitaxial PZT with GaN grown on Al_2O_3 using buffer

* Corresponding author.
E-mail address: g.koster@utwente.nl (G. Koster).

http://dx.doi.org/10.1016/j.tsf.2015.07.069
0040-6090/

layers such as MgO [20], TiO_2, $SrTiO_3$ [22], PbO, $PbTiO_3$ (with the epitaxial relationship PZT[11$\bar{2}$]||GaN[1$\bar{1}$00] and PZT[1$\bar{1}$0]||GaN[11$\bar{2}$0]) [26].

The R-TiO_2 buffer layer is expected to relieve the lattice mismatch between PZT and GaN because of the rutile crystal structure and the lattice constants of the R-TiO_2 (a = 4.58 Å and c = 2.95 Å) [28] match both GaN (a = 3.18 Å, c = 5.18 Å) [29] and PZT (a = 4.058 Å and c = 4.106 Å) [30]. Moreover, R-TiO_2 has a wide band gap of ~3 eV and a high dielectric constant [31] which makes this study also interesting in view of power transistor applications. The R-TiO_2 thin film is rather stable in contrast to water-soluble MgO and MgCaO thin films [32,33]. Here, the epitaxial growth of R-TiO_2 buffer layers on GaN was realized by using the pulsed laser deposition (PLD) method [27].

This paper focuses on a detailed study of the integration of PZT with commercially available substrates on which GaN was grown on Si (111) using optimized R-TiO_2 buffer layers. We first focus on the optimization of the growth morphology of the R-TiO_2 buffer layer grown by PLD on GaN (0002)/Si by adjusting the substrate temperature (T_s) and the oxygen pressure (pO_2). Subsequently, PZT films were grown on GaN/Si using the optimized TiO_2 buffered GaN/Si. The surface morphologies of the PZT/GaN/Si and the PZT/TiO_2/GaN/Si structures are investigated by AFM. We also compare the ferroelectric properties of PZT films grown on buffered and non-buffered GaN/Si substrates by using interdigitated-electrode (IDT) structures, fabricated on PZT/TiO_2/GaN/Si and PZT/GaN/Si stacks, respectively.

2. Methods

Ferroelectric PZT films and TiO_2 buffer layers were grown on GaN (0002) templated Si (111) substrates. The GaN templated Si (111) substrates include an $Al_xGa_{1-x}N$/GaN stack (see Fig. 2) forming a 2DEG at the $Al_xGa_{1-x}N$/GaN interface. The $Al_xGa_{1-x}N$ is covered with a 3 nm GaN cap layer.

First, before introducing the GaN/Si substrates in the PLD vacuum system, the surfaces were cleaned with acetone and ethanol. Next, R-TiO_2 thin films were grown on GaN/Si at T_s = 700 °C by the PLD and the oxygen pressure was varied between 10 Pa to 1 Pa, to find the optimal growth pressure. Subsequently, to find the optimal growth temperature, the T_s was varied from 600 °C to 700 °C. After obtaining an maximum amount of (200) oriented R-TiO_2 buffer layer (20 nm), a 300 nm PZT film was subsequently deposited on the R-TiO_2/GaN/Si stack using PLD and compared to a 300 nm PZT film grown on non-buffered GaN/Si. For the growth of the TiO_2 thin films we used a KrF (λ = 248 nm) excimer laser focussed on a Ti target and for PZT a pressed pellet with a composition close to that of morphotropic $Pb(Zr_{0.52}Ti_{0.48})O_3$ was used as a target. Further PLD growth details are summarized in Table 1. The crystal orientation of the TiO_2 films were investigated by X-ray diffraction (XRD) θ–2θ scans using a Panalytical X'PERT MPD. The X-ray source is a ceramic X-ray tube with Cu anode and normal operating power is 1.8 kW (45 kV, 40 mA). The in-plane epitaxial relationship between PZT and GaN was analyzed by XRD Φ scans (XRD, Bruker D8 Discover) with a Cu K_α cathode in the Bragg–Brentano geometry. The growth process of the R-TiO_2 films was monitored *in situ* by reflection high-energy electron diffraction (RHEED). The thickness of the film was obtained using a high-resolution scanning electron microscopy (HRSEM: Zeiss-1550), and the surface chemical properties were investigated by employing X-ray photoelectron spectroscopy (XPS) using an Omicron nanotechnology GmbH (Oxford Instruments) Surface Analysis system, having a background pressure of 5×10^{-9} Pa. The XPS system uses Al Kα X-ray radiation of 1486.7 eV. In addition, the surface morphologies of the GaN/Si, R-TiO_2 grown on GaN/Si, PZT grown on GaN/Si, and PZT grown on TiO_2 buffered GaN/Si were characterized by atomic force microscope (Bruker ICON Dimension AFM).

To measure the electrical performance of PZT films, IDT contacts were fabricated using Pt electrodes, which were sputter deposited on the PZT films. Finally, polarization-electric field (*P–E*) and switching current measurements were carried out to observe the effect of the buffer layer on the ferroelectric characteristics of PZT films using the ferroelectric mode of the AixACCT TF-2000 Analyzer.

Table 1
PLD growth parameters of PZT and R-TiO_2 films grown on GaN/Si.

Parameters	TiO_2	PZT
Ambient pressure	2 (O_2) Pa	10 (O_2) Pa
Energy density	2.0 J/cm^2	3.5 J/cm^2
Deposition temperature	675 °C	600 °C
Laser pulse frequency	2 Hz	4 Hz
Target to substrate distance	55 mm	60 mm
Deposition rate	0.02 nm/s	0.16 nm/s

3. Results and discussion

3.1. Growth and characterization of the PLD deposited R-TiO_2 films

Fig. 1 shows the θ–2θ scans of the layers that were deposited. Next to the expected Si(111), GaN(0002), and $Al_xGa_{1-x}N$(0002) peaks the results indicate that R-TiO_2 thin films with (200) orientation are obtained at 2 Pa oxygen pressure. For other pressures, R-TiO_2 thin films were not obtained. As shown in Fig. 1(b), R-TiO_2 thin film peaks were not observed in films using T_s values below 650 °C. Whereas the intensity of the (200) oriented R-TiO_2 peak starts to reduce at T_s values higher than 675 °C. Optimal crystallinity for R-TiO_2 is found at Ts = 675 °C and in pO_2 = 2 Pa by using a laser energy of 2.0 J/cm^2 as the (200) oriented XRD peak has become sharper (see Fig. 1(a) and (b)). When the oxygen pressure was lowered to 0.01 mbar, no rutile or anatase phase was observed. Apparently, the oxygen pressure has a strong effect

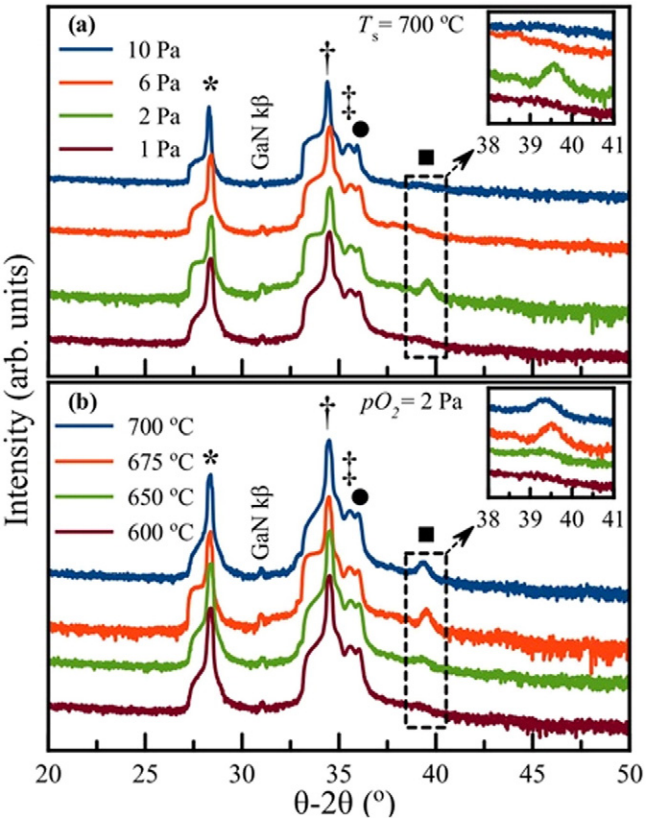

Fig. 1. XRD θ–2θ scans of 20 nm R-TiO_2 thin films deposited on GaN/Si (a) for different oxygen pressures at T_s = 700 °C and (b) for different substrate temperatures under pO_2 = 2 Pa. The diffraction peaks of different layers are marked with different symbols: * is Si, † is GaN (0002), ‡ is $Al_{0.20}Ga_{0.80}N$, ● is AlN (0002) and ▪ is R-TiO_2 (200). For clarity the R-TiO_2 peaks have been magnified in the insets of both figures.

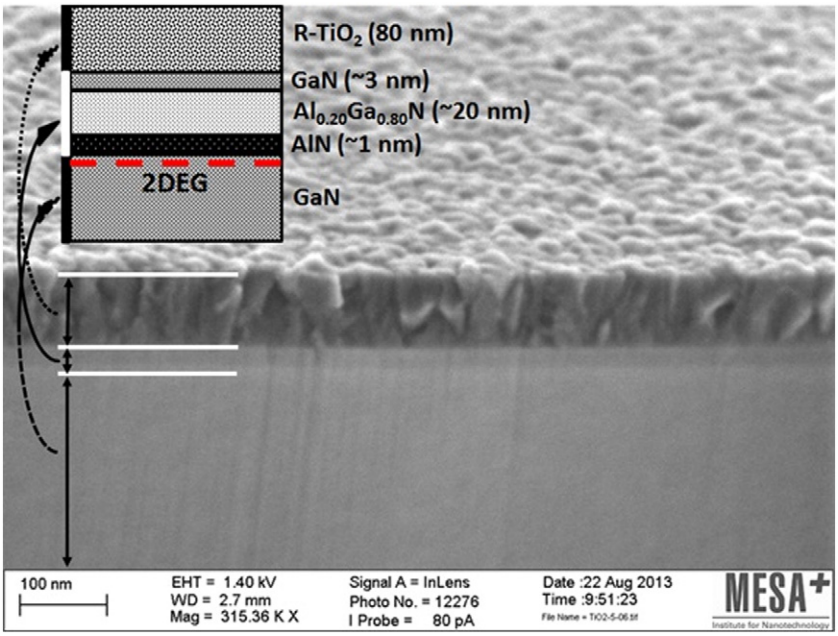

Fig. 2. Cross-sectional HR-SEM image of an R-TiO_2 thin film grown on GaN/Si.

on the stoichiometry of the films which in turn affects the nucleation density and film quality. Hence, the films remain non-stoichiometric at low oxygen pressures [34]. These results show that the optimized temperature and pressure values given above are critical parameters to obtain R-TiO_2 thin films on the GaN/Si substrates. The deposition rate of R-TiO_2 grown at 2 Pa O_2 at 675 °C by using a laser energy of 2.0 J/cm^2 at 4 Hz for 60 min is estimated to be around 0.02 nm/s. This value was obtained from the HR-SEM image (Fig. 2).

The optimized growth conditions of (100) oriented R-TiO_2 films grown on GaN/Si are summarized in Table 1. The surface morphology of the GaN/Si surface and R-TiO_2 films on the GaN/Si surface was investigated by AFM and RHEED, as shown in Fig. 3. The original GaN (0002)/Si (111) surface shows two dimensional (2D) RHEED patterns along the [11$\bar{2}$0] azimuth while the surface of a 20 nm R-TiO_2 thin film on GaN/Si shows three dimensional (3D) RHEED patterns along the [001] azimuth.

The lattice mismatch of ~20% between the R-TiO_2 film and GaN can lead to 3D island growth formation [35,36]. The increase of the R-TiO_2 film thickness results in an increase in the overall strain in the film during deposition. The AFM root mean square (rms) values of the GaN/Si surface roughness and that of the 20 nm thick R-TiO_2 on GaN/Si are 0.10 nm and 0.52 nm, respectively. The surface of the 20 nm thin R-TiO_2 on GaN/Si exhibits small grains due to the 3D island formation during the growth, as shown in Fig. 3(b).

Finally, the R-TiO_2 film surface has been investigated by XPS. Fig. 4(a) shows the typical spectra of Ti^{4+} in TiO_2. The Ti $2p_{3/2}$ and Ti $2p_{1/2}$ photoelectron peaks, corresponding to a pure R-TiO_2 film, are located at 459.4 eV and 465.2 eV, respectively [37]. The spin-orbital splitting between Ti $2p_{3/2}$ and Ti $2p_{1/2}$ peaks is as expected constant at approximately 5.8 eV. In the inset of Fig. 4(a), the Ti $2p_{3/2}$ low-binding-energy shoulder around 458 eV indicates the presence of oxidized Ti states. Also, in the O 1s spectra the binding energies at 529.6 eV and 530.9 eV correspond to oxygen bound to Ti^{4+} ions in TiO_2 and oxygen deficient TiO_2 ($Ti^{3+/4+}$), respectively [38]. The binding energy at 531.9 eV indicates that the surface is partially covered with hydroxide OH groups after having been exposed to air. Note that the carbon signal also arises because the TiO_2 film was exposed to air after deposition, see Table 2.

The XPS spectra of Ti 2p in TiO_2 did not show Ti^{3+} and Ti^{2+} photoelectron signals corresponding to the possible formation of Ti_2O_3 and TiO. This means that the composition of the surface layer is TiO_2 and not a mixture of different oxides with an average Ti/O ratio of 1:2 and consistent with the rutile phase of TiO_2.

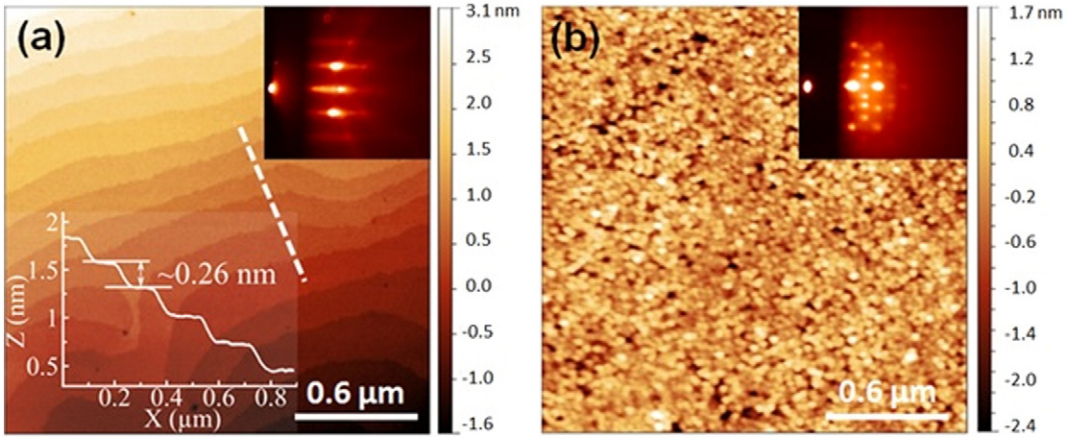

Fig. 3. The surface morphology of (a) the GaN surface and (b) 20 nm R-TiO_2 grown on GaN/Si. Inset (a): RHEED patterns of GaN (0002) along the [11$\bar{2}$0] azimuth and line profile along white dashed line. Inset (b): RHEED patterns of 20 nm thin TiO_2 film grown on GaN/Si along the [001] azimuth.

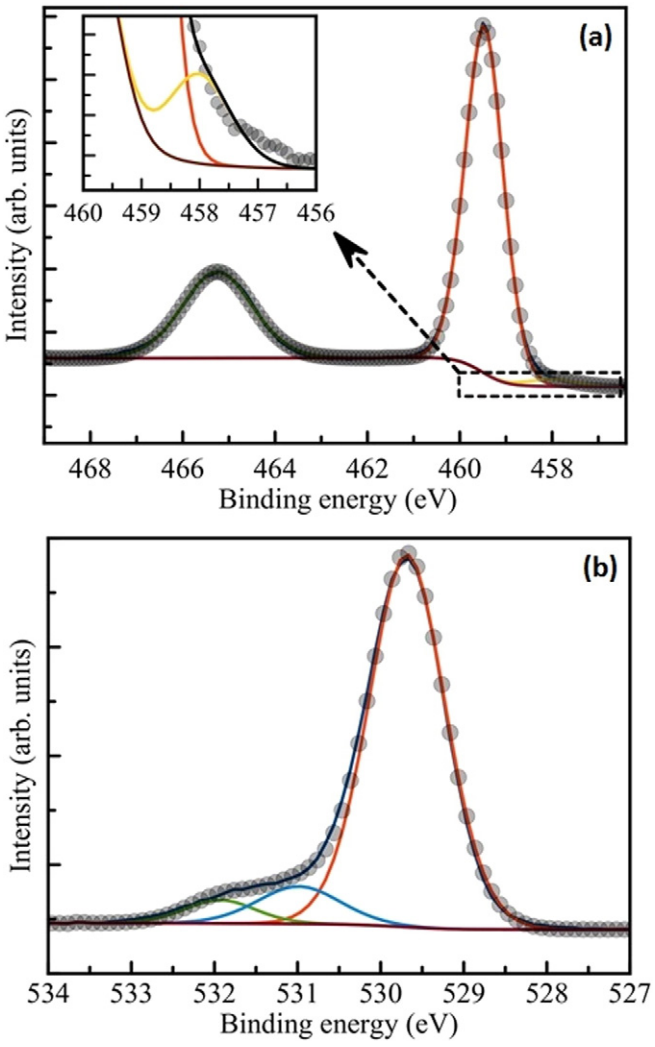

Fig. 4. Core level spectra of the R-TiO_2 thin film of (a) Ti 2p (inset: low-binding-energy shoulder in the Ti $2p_{3/2}$ peak) and (b) O 1s.

Summarizing, (100) R-TiO_2 thin films were obtained on GaN (0002)/Si (111) using PLD. Unlike the growth conditions of R-TiO_2 thin films grown on GaN/Al_2O_3 (500 °C ≤ T_s ≤ 600 °C, 1×10^{-4} Pa ≤ pO_2 ≤ 1.3×10^{-3} Pa) reported in [27] and [35], in our work, R-TiO_2 thin films grown on GaN/Si were obtained at $T_s \geq 675$ °C and in $pO_2 = 2$ Pa. The growth morphology of R-TiO_2 thin films grown on GaN/Si was investigated. Thicker TiO_2 films showed 3D island formation. The chemical composition corresponding to pure R-TiO_2 was detected by XPS, with some oxygen deficiency, which was also confirmed by XRD showing that the TiO_2 film has the rutile structure. It has been previously shown that the preferred orientation of the PZT films can be maintained using relatively thick buffer layers [39]. Moreover, the thickness of the TiO_2 buffer layer between PZT and a substrate has been shown to be an important parameter to control the amount of diffused Pb into the substrate [40] as well as reducing leakage. Therefore, in the following experiments, in order to prevent the diffusion of

Table 2
The atomic concentrations of different elements at the R-TiO_2 surface.

Elements	% concentr.
Ti 2p	25
O 1s	53
C 1s	23

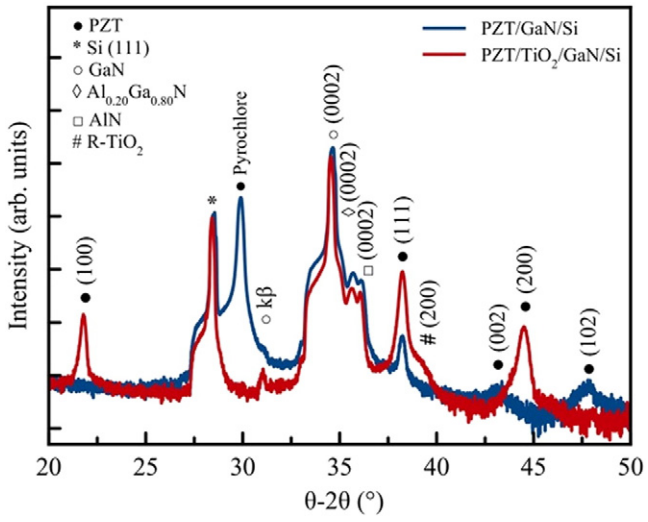

Fig. 5. XRD θ–2θ scans of the PZT/GaN/Si and PZT/TiO_2/GaN/Si structures. The thicknesses of the R-TiO_2 and PZT films are 20 nm and 300 nm, respectively. The diffraction peaks of different layers are marked with different symbols in figure.

Pb into GaN/Si during the PZT deposition, a 20 nm R-TiO_2 buffer layer was used.

3.2. Deposition of PZT films on R-TiO_2 buffered GaN templated Si (111)

In order to investigate the effect of the R-TiO_2 buffer layer on the growth of PZT, we now compare PZT films directly deposited on GaN/Si and on R-TiO_2 buffered GaN/Si substrates.

Fig. 5 shows the XRD θ–2θ measurements for the PZT/GaN/Si and PZT/TiO_2/GaN/Si structures. The PZT and TiO_2 layer thickness is 300 nm

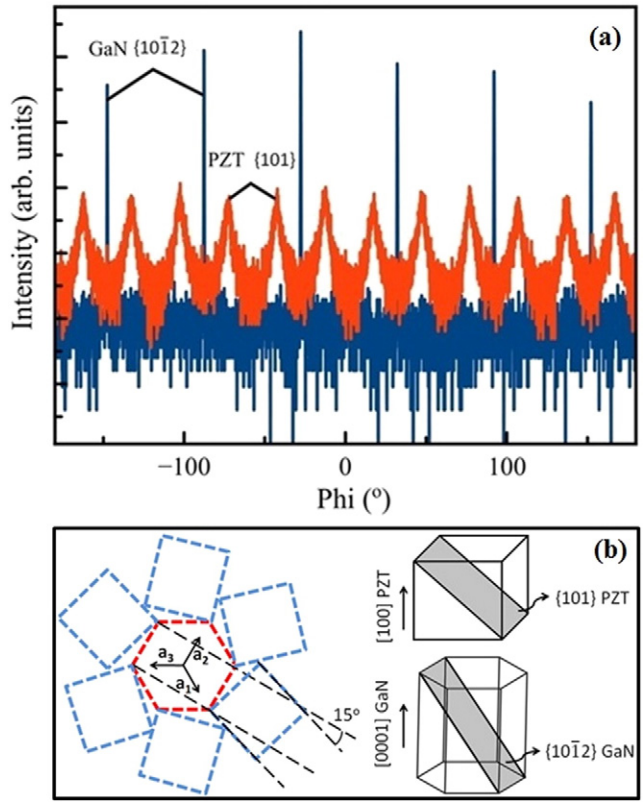

Fig. 6. (a) XRD Φ scans of the {101} PZT and {10$\bar{1}$2} GaN reflections of the PZT/TiO_2/GaN/Si structure. (b) Schematic top view of the unit cell configuration of PZT on GaN.

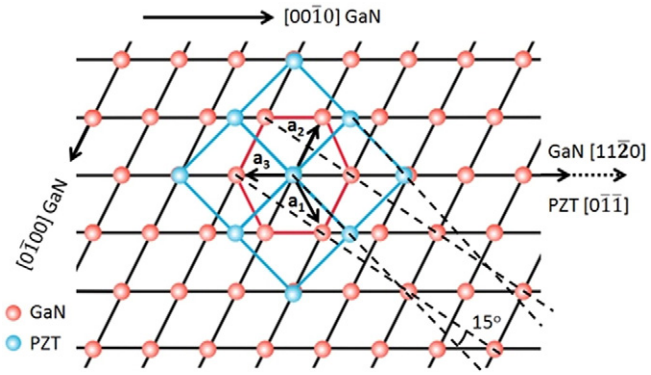

Fig. 7. Schematic of in-plane orientation of (100) oriented PZT on (0002) GaN.

and 20 nm, respectively. The results show that a PZT thin film with (100) and (111) orientation was obtained on the TiO_2/GaN/Si(111) substrates, without the appearance of a detectable amount of the pyrochlore phase. In contrast, the pyrochlore phase was observed in the PZT film directly grown on the GaN/Si(111) substrate. The growth parameters of PZT are summarized in Table 1. The rocking curve (not shown here) of the (111) oriented PZT film has a full width at half maximum (FWHM) of 1.86°, which is lower compared to earlier reports [20].

XRD Φ scans have been carried out to study the in-plane epitaxial relationship between the PZT and the GaN. The in-plane alignment of the PZT films grown on R-TiO_2 buffered GaN is confirmed by the scans of PZT {101} and GaN {10$\bar{1}$2} reflections shown in Fig. 6(a). The diffraction peaks of {1012} plane of GaN, observed at every 60°, show that GaN epilayer has a sixfold symmetry indicating its wurtzite structure. However, twelve diffraction peaks of PZT {101} are separated by 30°. Note that in these scans the R-TiO_2 peaks do not show because of low intensity. For clarity, a schematic of PZT on GaN is shown Fig. 6(b). These Φ-scans can be interpreted that the PZT film grow epitaxially on TiO_2 buffered GaN, with the epitaxial relationship (100)[0$\bar{1}\bar{1}$]PZT// (0002)[11$\bar{2}$0]GaN. A schematic illustration of the epitaxial orientation relationship between (100) PZT and (0002) GaN is shown in Fig. 7.

The surface morphologies revealed by AFM of 300 nm thick PZT films grown on GaN/Si and R-TiO_2 buffered GaN/Si are shown in Fig. 8(a) and (b), respectively. The roughness of PZT film grown on GaN/Si (rms: 3.31 nm) is lower than that of a PZT film grown on R-TiO_2 buffered GaN/Si (rms: 7.13 nm), and both these films demonstrate a grainy structure. Fig. 8(b) shows relatively bigger crystalline PZT islands, grain size of ~150 nm, with an irregular shape form, compared to PZT grown

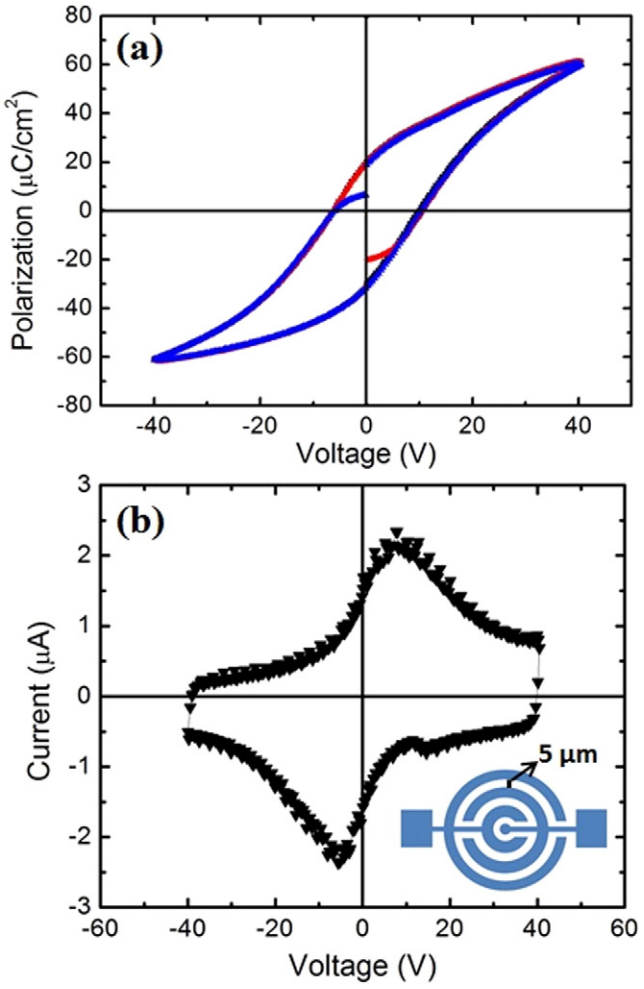

Fig. 9. (a) The *P–E* loop and (b) switching current characteristics of the PZT/TiO_2/GaN/Si heterostructure measured with an IDT structure (for top view, see inset) at 1 kHz.

on GaN/Si (see Fig. 8(a)). The AFM results indicate that the R-TiO_2 buffer layer plays an important role on the surface morphology and grain size of the PZT films.

Finally, in order to investigate the ferroelectric properties of PZT films grown on GaN/Si and TiO_2/GaN/Si substrates, an IDT structure was fabricated on the surface of the PZT film, as shown in the inset of Fig. 9. The IDT electrodes were used to achieve the d_{33}-mode of operation. In this mode the applied electric field and the ferroelectric

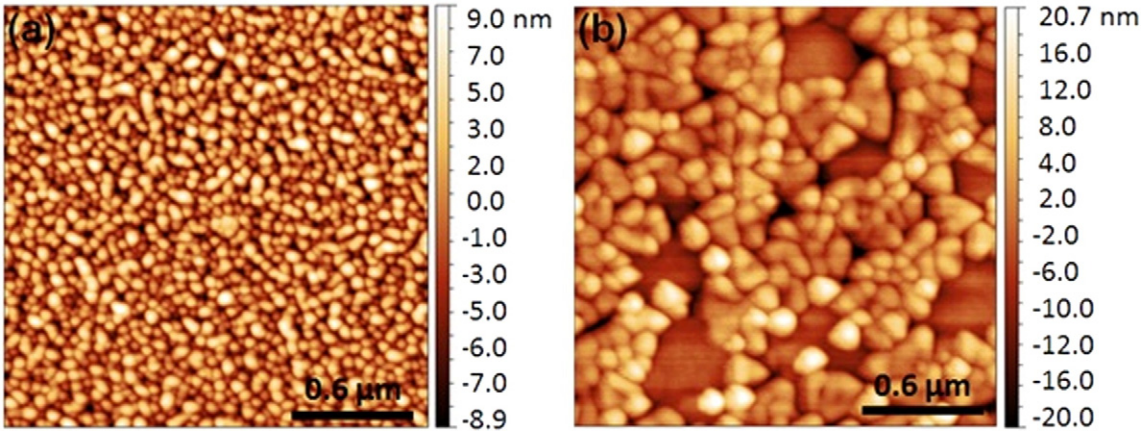

Fig. 8. The surface morphology of (a) 300 nm PZT grown on GaN/Si and (b) 300 nm PZT grown on R-TiO_2 buffered GaN/Si.

polarization are along the PZT film surface [41]. Thus, the PZT films are poled in the plane of the film [42]. An electrode consisting of 100 nm thick Pt layer was deposited by using sputter deposition. The results indicate that the PZT film on GaN/Si does not appear to be ferroelectric (not shown here). This is caused by an irreproducible high leakage current which prevents the formation of a closed polarization-electric field (*P*–*E*) loop. On the other hand, the PZT film grown on TiO_2/GaN/Si shows ferroelectric behavior as demonstrated with a characteristic hysteretic *P*–*E* curve, as shown in Fig. 9(a). The remnant polarization (P_r) and coercive voltage (V_c) of the PZT film grown on TiO_2/GaN/Si are 25.6 μC/cm^2 and 8.1 V, respectively. Fig. 8(b) shows that PZT films grown on TiO_2/GaN/Si can be switched in two directions. Earlier reports showed that the PZT films grown on GaN/Al_2O_3 exhibit ferroelectric properties, although the pyrochlore phase was observed [20,23,43]. In contrast with these earlier reports, we found that the PZT films grown directly on GaN/Si appear to not exhibit ferroelectric properties concealed by the high leakage currents.

4. Conclusions

It has been shown that optimized (100) oriented R-TiO_2 buffer layers can be grown on GaN/Si (111) at $T_s = 675$ °C and in $pO_2 = 2$ Pa by using PLD. Both these T_s and pO_2 values are higher than that of R-TiO_2 thin films grown on GaN/Al_2O_3 reported earlier [27, T_s = 500–600 °C, $pO_2 = 1 \times 10^{-4}$ Pa]. By using RHEED, a 3D island growth formation was observed for the 20 nm thin R-TiO_2 film. It has also been shown that a PZT film grown directly on GaN/Si shows the pyrochlore phase, while the R-TiO_2 buffer layer on GaN prevented this. The R-TiO_2 buffer layer enabled the growth of epitaxial PZT films on GaN/Si, and effectively promoted the growth of ferroelectric PZT films, as confirmed in the *P*–*E* loop measurements.

Acknowledgments

This work has been supported by NanoNextNL under Project No. NNNL-07B.04.

References

[1] L. Hao, J. Zhu, Y. Liu, S. Wang, H. Zeng, X. Liao, Y. Liu, H. Lei, Y. Zhang, W. Zhang, Y. Li, Integration and electrical properties of epitaxial $LiNbO_3$ ferroelectric film on n-type GaN semiconductor, Thin Solid Films 520 (2012) 3035.
[2] A.J. Bell, Factors influencing the piezoelectric behaviour of PZT and other "morphotropic phase boundary" ferroelectrics, J. Mater. Sci. 41 (2006) 13.
[3] A. Kumar, A. Rao, M. Goswami, B.R. Singh, Electrical characterization of MFeOS gate stacksfor ferroelectric FETs, Mater. Sci. Semicond. Process. 16 (2013) 1603.
[4] U. Schroeder, S. Mueller, J. Mueller, E. Yurchuk, D. Martin, C. Adelmann, T. Schloesser, R. van Bentum, T. Mikolajick, Hafnium oxide based CMOS compatible ferroelectric materials, ECS J. Solid State Sci. Technol. 2 (2013) N69–N72.
[5] M. Klee, D. Wissen, W. Keur, R. Kiewitt, D. Bausen, P. Lok, Oxide films for integrated capacitors in thin film functional modules, Proc. Mater. Res. Soc. Symp. 655 (2001) CC13.1.11.
[6] N. Setter, D. Damjanovic, L. Eng, G. Fox, S. Gevorgian, S. Hong, A. Kingon, H. Kohlstedt, N.Y. Park, G.B. Stephenson, I. Stolitchnov, A.K. Taganstev, D.V. Taylor, T. Yamada, S. Streiffer, Ferroelectric thin films: review of materials, properties, and applications, J. Appl. Phys. 100 (2006) 051606.
[7] C. A-Paz de Araujo, J.D. Cuchiaro, L.D. McMillan, M.C. Scott, J.F. Scott, Fatigue-free ferroelectric capacitors with platinum electrodes, Nature 374 (1995) 627.
[8] S. Salahuddin, S. Datta, Use of negative capacitance to provide voltage amplification for low power nanoscale devices, Nano Lett. 8 (2008) 405.
[9] A. Rusu, G.A. Salvatore, D. Jimenez, A.M. Ionescu, Metal–ferroelectric–metal–oxide–semiconductor field effect transistor with sub-60 mV/decade subthreshold swing and internal voltage amplification, Int. Electr. Dev. Meet. 395 (2010) 16.3.1.
[10] T. van Hemert, R.J.E. Hueting, Piezoelectric strain modulation in FETs, IEEE Trans. Electron Devices 60 (2013) 3265.
[11] B. Kaleli, R.J.E. Hueting, M.D. Nguyen, R.A.M. Wolters, Analysis of thin-film PZT/LNO stacks on an encapsulated TiN electrode, IEEE Trans. Electron Devices 61 (2014) 119.
[12] Y. Cao, G. Sheng, J.X. Zhang, S. Choudhury, Y.L. Li, C.A. Randall, L.Q. Chen, Piezoelectric response of single-crystal $PbZr_{1-x}Ti_xO_3$ near morphotropic phase boundary predicted by phase-field simulation, Appl. Phys. Lett. 97 (2010) 252904.
[13] N. Vittayakorn, G. Rujijanagul, X. Tan, M.A. Marquardt, D.P. Cann, The morphotropic phase boundary and dielectric properties of the $xPb(Zr_{1/2}Ti_{1/2})O_3$-$(1-x)Pb(Ni_{1/3}Nb_{2/3})O_3$ perovskite solid solution, J. Appl. Phys. 96 (2004) 5103.
[14] S. Nakamura, T. Mukai, M. Senoh, High-power GaN P–N junction blue-light-emitting diodes, Jpn. J. Appl. Phys. 30 (1991) L1998.
[15] L.F. Eastman, U. Mishra, The toughest transistor yet [GaN transistors], IEEE Spectr. 39 (2002) 28.
[16] U. Mishra, L. Shen, T. Kazior, Y.-F. Wu, GaN-based RF power devices and amplifiers, Proc. IEEE 96 (2008) 287.
[17] K. Elibol, G. Atmaca, P. Tasli, S.B. Lisesivdin, A numerical study on subband structure of $In_xAl_{1-x}N$/GaN-based HEMT structures with low-indium ($x < 0.10$) barrier layer, Solid State Commun. 162 (2013) 8.
[18] M. Van Hove, S. Boulay, S.R. Bahl, S. Stoffels, X. Kang, D. Wellekens, K. Geens, A. Delabie, S. Decoutere, CMOS process-compatible high-power low-leakage AlGaN/GaN MISHEMT on silicon, Electron. Dev. Lett. 33 (2012) 667.
[19] M. Jamil, J.R. Grandusky, V. Jindal, N. Tripathi, F. Shahedipour-Sandvik, Mechanism of large area dislocation defect reduction in GaN layers on AlN/Si (111) by substrate engineering, J. Appl. Phys. 102 (2007) 023701.
[20] E.A. Paisley, H.S. Craft, M.D. Losego, H. Lu, A. Gruverman, R. Collazo, Z. Sitar, J.-P. Maria, Epitaxial lead zirconate titanate on gallium nitride, J. Appl. Phys. 113 (2013) 074107.
[21] J. Zhang, C. Yang, S. Wu, Y. Liu, M. Zhang, H. Chen, W. Zhang, Y. Li, Tuning two-dimensional electron gas of ferroelectric/GaN heterostructures by ferroelectric polarization, Semicond. Sci. Technol. 25 (2010) 035011.
[22] Y. Li, J. Zhu, W. Luo, Study of the integrated growth of dielectric films on GaN semiconductor substrates, IEEE-UFFC 57 (2010) 2192.
[23] A. Gruverman, W. Cao, S. Bhaskar, S.K. Dey, Investigation of Pb(Zr, Ti)O3/GaN heterostructures by scanning probe microscopy, Appl. Phys. Lett. 84 (2004) 5153.
[24] S.K. Dey, W. Cao, S. Bhaskar, J. Li, Highly textured $Pb(Zr_{0.3}Ti_{0.7})O_3$ thin films on GaN/sapphire by metalorganic chemical vapor deposition, J. Mater. Res. 21 (2006) 1526.
[25] E.S. Lee, H.W. Chung, S.H. Lim, S.Y. Lee, Effect of double-sided $(Pb_{0.72}La_{0.28})Ti_{0.93}O_3$ buffer layers on the ferroelectric properties of $Pb(Zr_{0.52}Ti_{0.48})O_3$ thin films, Appl. Phys. Lett. 86 (2005) 032903.
[26] B. Xiao, X. Gu, N. Izyumskaya, V. Avrutin, J. Xie, H. Liu, H. Morkoç, Structural and electrical properties of Pb(Zr, Ti)O_3 grown on (0001) GaN using a double $PbTiO_3$/PbO bridge layer, Appl. Phys. Lett. 91 (2007) 182908.
[27] F. Mei, X. Xiao, J. Xu, Y. Zhou, D. Zhang, Heteroepitaxial growth and structural characterization of rutile TiO_2 thin films on GaN (0001) templates prepared by pulsed laser deposition, Nucl. Inst. Methods Phys. Res. B 307 (2013) 477.
[28] Ta-Chang Tien, Fu-Ming Pan, Lih-Ping Wang, Feng-Yu. Tsai, Ching Lin, Growth mode transition of atomic layer deposited Al_2O_3 on porous TiO_2 electrodes of dye-sensitized solar cells, Thin Solid Films 520 (2012) 1745.
[29] V. Darakchieva, P.P. Paskov, T. Paskova, E. Valcheva, B. Monemar, M. Heuken, Lattice parameters of GaN layers grown on a-plane sapphire: effect of in-plane strain anisotropy, Appl. Phys. Lett. 82 (2003) 703.
[30] M.D. Nguyen, M. Dekkers, E. Houwman, R. Steenwelle, X. Wan, A. Roelofs, T. Schmitz-Kempen, G. Rijnders, Misfit strain dependence of ferroelectric and piezoelectric properties of clamped (001) epitaxial Pb(Zr0.52, Ti0.48)O3 thin films, Appl. Phys. Lett. 99 (2011) 252904.
[31] U. Diebold, The surface science of titanium dioxide, Surf. Sci. Rep. 48 (2003) 53.
[32] K. Okimura, T. Furumi, In-plane orientation and annealing behavior of rutile TiO_2 films on MgO substrate prepared by inductively coupled plasma-assisted sputtering, Jpn. J. Appl. Phys. 44 (2005) 3192.
[33] B.P. Gila, M. Hlad, A.H. Onstine, R. Frazier, G.T. Thaler, A. Herrero, E. Lambers, C.R. Abernathy, S.J. Pearton, T. Anderson, S. Jang, F. Ren, N. Moser, R.C. Fitch, M. Freund, Improved oxide passivation of AlGaN/GaN high electron mobility transistors, Appl. Phys. Lett. 87 (2005) 163503.
[34] A. Ohtomo, H.Y. Hwang, Growth mode control of the free carrier density in $SrTiO_{3-\delta}$ δ films, J. Appl. Phys. 102 (2007) 083704.
[35] T. Hitosugi, Y. Hirose, J. Kasai, Y. Furubayashi, M. Ohtani, K. Nakajima, T. Chikyow, T. Shimada, T. Hasegawa, Heteroepitaxial growth of rutile TiO_2 on GaN(0001) by pulsed laser deposition, Jpn. J. Appl. Phys. 44 (2005) L1503.
[36] W.B. Luo, J. Zhu, C.G. Wu, Y. Shuai, W.L. Zhang, Y. Zhang, S. Zhou, S. Gemming, H. Schmidt, Effects of the TiO_2 buffer thickness on $SrTiO_3$ (111) epitaxial films grown on GaN (0002), J. Appl. Phys. 113 (2013) 154103.
[37] W. Hu, Y. Liu, R.L. Withers, T.J. Frankcombe, L. Norén, A. Snashall, M. Kitchin, P. Smith, B. Gong, H. Chen, J. Schiemer, F. Brink, J. Leung, Electron-pinned defect-dipoles for high-performance colossal permittivity materials, Nat. Mater. 12 (2013) 821.
[38] J. Fang, X. Bi, D. Si, Z. Jiang, W. Huang, Spectroscopic studies of interfacial structures of CeO_2–TiO_2 mixed oxides, Appl. Surf. Sci. 253 (2007) 8952.
[39] H. Kim, J.H. Kim, W.K. Choo, Effects of $LaNiO_3$ buffer layer thickness on the ferro- and piezoelectric properties of PZT films, Integr. Ferroelectr. 64 (2004) 125.
[40] A. Bose, M. Sreemany, S. Bysakh, Role of TiO_2 seed layer thickness on the nanostructure evolution and phase transformation behavior of sputtered PZT thin films during post-deposition air-annealing, J. Am. Ceram. Soc. 94 (2011) 4066.
[41] B. Xu, Y. Ye, L.E. Cross, J.J. Bernstein, R. Miller, Dielectric hysteresis from transverse electric fields in lead zirconate titanate thin films, Appl. Phys. Lett. 74 (1999) 3549.
[42] H.G. Yu, L. Zou, K. Deng, R. Wolf, S. Tadigadapaa, S. Trolier-McKinstry, Lead zirconate titanate MEMS accelerometer using interdigitated electrodes, Sensors Actuators A 107 (2003) 26.
[43] W. Cao, S. Bhaskar, J. Li, S.K. Dey, Interfacial nanochemistry and electrical properties of $Pb(Zr_{0.3}Ti_{0.7})O_3$ films on GaN/sapphire, Thin Solid Films 484 (2005) 154.